A Conformational Dynamics Study of α-L-Rha*p*-(1→2)[α-L-Rha*p*-(1→3)]-α-L-Rha*p*-OMe in Solution by NMR Experiments and Molecular Simulations

Robert Eklund, Kristina Lycknert, Peter Söderman, and Göran Widmalm*

Department of Organic Chemistry, Arrhenius Laboratory, Stockholm University, S-106 91 Stockholm, Sweden

Received: June 14, 2005; In Final Form: August 16, 2005

The conformational preference of α-L-Rha*p*-(1→2)[α-L-Rha*p*-(1→3)]-α-L-Rha*p*-OMe in solution has been studied by NMR spectroscopy using one-dimensional ^{1}H,^{1}H T-ROESY experiments and measurement of trans-glycosidic $^3J_{C,H}$ coupling constants. Molecular dynamics (MD) simulations with a CHARMM22 type of force field modified for carbohydrates were performed with water as the explicit solvent. The homonuclear cross-relaxation rates, interpreted as effective proton−proton distances, were compared to those obtained from simulation. Via a Karplus torsional relationship, $^3J_{C,H}$ values were calculated from simulation and compared to experimental data. Good agreement was observed between experimental data and the MD simulation, except for one inter-residue T-ROE between protons in the terminal sugar residues. The results show that the trisaccharide exhibits substantial conformational flexibility, in particular along the ψ glycosidic torsion angles. Notably, for these torsions, a high degree of correlation (77%) was observed in the MD simulation revealing either ψ_2^+ ψ_3^+ or $\psi_2^-\psi_3^-$ states. The simulations also showed that non-exoanomeric conformations were present at the ϕ torsion angles, but to a limited extent, with the ϕ_3 state populated to a larger extent than the ϕ_2 state. Further NMR analysis of the trisaccharide by translational diffusion measurements and ^{13}C T_1 relaxation experiments quantified global reorientation using an anisotropic model together with interpretation of the internal dynamics via the "model-free" approach. Fitting of the dynamically averaged states to experimental data showed that the $\psi_2^+\psi_3^+$ state is present to ∼49%, ψ_2^- ψ_3^- to ∼39%, and ϕ_3 (non-exo) to ∼12%. Finally, using a dynamic and population-averaged model, ^{1}H,^{1}H T-ROE buildup curves were calculated using a full relaxation matrix approach and were found to be in excellent agreement with experimental data, in particular for the above inter-residue proton−proton interaction between the terminal residues.

Introduction

Cell surface interactions are complex processes where protein−protein and carbohydrate−protein[1] recognition events are important for signaling and trafficking. Moreover, carbohydrate−carbohydrate[2] interactions may also play an important role in these processes even though they are weak. The latter are substantially enhanced by multivalency modes of action. The carbohydrate part of glycoproteins and glycolipids shows a large structural diversity, and modifications of it can be utilized in processes where regulation is essential.[3]

The three-dimensional shape of an oligosaccharide should therefore be described in the greatest detail possible. In isotropic solution, the nuclear Overhauser effect (NOE) observed by NMR spectroscopy experiments has been of utmost importance. More recently, heteronuclear trans-glycosidic coupling constants have been added as complementary information.[4] Also, hydroxyl protons of sugars have been useful for reporting on conformational preferences. The latter studies have usually been performed with the aprotic solvent DMSO,[5] but sometimes with water mixed with acetone,[6] or with supercooled water.[7] Other recent developments include the use of dilute lyotropic liquid crystal phases, in which NMR residual dipolar couplings from the saccharide can be measured and thereby supply additional information on carbohydrate conformation,[8,9] but they can be hard to interpret since the lyotropic crystalline phase may interact too strongly with the solute molecule and thereby change the populations of the conformational equilibrium.[10]

* Corresponding author. E-mail: gw@organ.su.se.

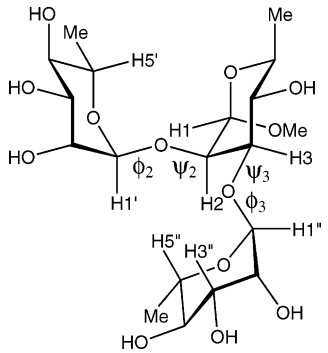

Figure 1. Schematic of trisaccharide **1** with glycosidic torsion angles denoted as ϕ_2 to ψ_3.

In oligosaccharides, substitution with an additional sugar residue may change the conformation and dynamics of the adjacent residues. NMR ^{13}C chemical shifts are diagnostic in revealing conformational changes, in particular, upon vicinal disubstitution.[11] Although not formally branched, trisaccharides with vicinal substitution, compared with their disaccharide counterparts, are suitable models for the study of oligosaccharide conformation, which can be used to develop and evaluate methods to be applied to systems of higher complexity.

We have previously investigated the conformation and dynamics of different trisaccharides.[5,12] In the present study we analyze the trisaccharide α-L-Rha*p*-(1→2)[α-L-Rha*p*-(1→3)]-α-L-Rha*p*-OMe (**1**) shown in Figure 1, the constituent disaccharides of which we have earlier analyzed.[13] L-Rhamnose is a

10.1021/jp053198o CCC: $30.25
Published on Web 09/21/2005

common constituent of bacterial polysaccharides and α-(1→2)- and α-(1→3)-linkages between L-rhamnose residues are present in, for example, the O-antigen polysaccharides from *Shigella flexneri*,[14] *Shigella dysenteriae* type 1,[15] a *Klebsiella pneumoniae* strain,[16] and the cell-wall polysaccharide from *Streptococcus* group A. The conformational preference of the latter has been studied by molecular modeling and NMR spectroscopy on different oligosaccharides, in particular with the use of NOE-based experiments.[17,18] The branching region in this polysaccharide consists of α-L-Rha*p*-(1→2)[β-D-Glc*p*NAc-(1→3)]-α-L-Rha*p*. It should be noted that, in general, the overall conformational region of a β-D-hexopyranoside is similar to that of an α-L-hexopyranoside,[19] making a comparison of conformational and dynamic properties of the branch-point region in the *Streptococcus* group A polysaccharide to those in **1** of additional interest.

Some time ago, trisaccharide **1** was studied by NMR spectroscopy and molecular mechanics calculations in which NOE data were obtained by preirradiation of the anomeric protons in the terminal groups and energy minimization of the potential energy, respectively.[20] Interestingly, two conformations of similar potential energy were observed in which correlations between the ψ torsion angles were present, with the two ψ torsions having either positive or negative values. The alternative combinations for these torsions had higher potential energy and were not energetically accessible. It was concluded that the conformational freedom was somewhat restricted compared to **1**'s disaccharide counterparts, and that the conformational state with negative values of the two ψ torsions is present in aqueous solution.

Herein we show that even for a trisaccharide, the interpretation of conformation and flexibility is far from trivial, and we utilize NMR parameters in the analysis, viz., heteronuclear $^3J_{C,H}$ measurements, ^{1}H,^{1}H T-ROESY experiments, and ^{13}C T_1 relaxation measurements, in combination with Langevin dynamics (LD) and molecular dynamics (MD) simulations with explicit water as the solvent, to obtain information on the conformational dynamics of the system.

Theory

Proton−proton relaxation for molecules in solution is dominated by the dipole−dipole cross-relaxation between spins that are close in space. The strength of these interactions is dependent on the internuclear distance(s) and the dynamics of the molecule, both the internal and overall rotation. If a suitable reference proton−proton pair distance of known separation in the molecule is available, and the dynamics of the different proton pairs under considerations can be judged to be similar, the isolated spin-pair approximation (ISPA)[21,22] can be used by comparing the cross-relaxation rate of the reference spin pair, σ_{ref}, to that of protons i and j, σ_{ij}. Subsequently, the unknown distance, r_{ij}, between the protons can be obtained according to

$$r_{ij} = r_{ref}(\sigma_{ref}/\sigma_{ij})^{1/6} \tag{1}$$

The homonuclear dipolar relaxation for a molecule tumbling in solution can be described by[23−25]

$$\frac{d\mathbf{M}}{dt} = -\mathbf{R}\mathbf{M_0} \tag{2}$$

where **M** is a column matrix of values for the instantaneous magnetizations of the spins in the system, $\mathbf{M}_0$ is the column matrix of initial values for the magnetization of the spins in the system, and **R** is the relaxation matrix. For the nuclear Overhauser effect (NOE) measured in the laboratory frame,[26] the diagonal elements (ρ_{ii}) of **R** are given by

$$\rho_{NOE} = \frac{(d_{HH})^2}{4}[J(0) + 3J(\omega) + 6J(2\omega)] \tag{3}$$

where $J(\omega)$ is the spectral density function taken at different combinations of the proton frequency. The dipolar coupling constant, $d_{HH} = (\mu_0/4\pi)\gamma_H{}^2\hbar r^{-3}$, is a measure of the strength of the dipolar interaction, where μ_0 is the permeability in a vacuum, γ_H is the magnetogyric ratio for protons, $\hbar$ is Planck's constant divided by 2π, and r is the distance between interacting protons. The off-diagonal elements (σ_{ij}) describing the cross-relaxation rates are given by

$$\sigma_{NOE} = \frac{(d_{HH})^2}{4}[6J(2\omega) - J(0)] \tag{4}$$

In analogy, for the rotating-frame Overhauser effect (ROE),[27,28] the diagonal elements of **R** are given by

$$\rho_{ROE} = \frac{(d_{HH})^2}{8}[5J(0) + 9J(\omega) + 6J(2\omega)] \tag{5}$$

The off-diagonal elements describing the cross-relaxation rates are then given by

$$\sigma_{ROE} = \frac{(d_{HH})^2}{4}[3J(\omega) + 2J(0)] \tag{6}$$

In the multiple-pulse or transverse ROE (T-ROE), the cross-relaxation rate, σ_{T-ROE}, can be calculated as the mean of σ_{NOE} and σ_{ROE}, as described by[29−31]

$$\sigma_{T-ROE} = \frac{(d_{HH})^2}{8}[6J(2\omega) + 3J(\omega) + J(0)] \tag{7}$$

Equation 2 can be solved according to

$$\mathbf{M}(\tau_{mix}) = \chi \exp(-\lambda\tau_{mix})\chi^{-1}\mathbf{M_0} \tag{8}$$

where χ is the column matrix of eigenvectors of the relaxation matrix **R**, χ^{-1} is the inverse of χ, λ is the diagonal matrix of eigenvalues, and τ_{mix} is the mixing time. After diagonalization of the relaxation matrix **R**, using, for example, Cholesky factorization,[32] one obtains the eigenvector and eigenvalue matrixes of eq 8. Subsequently, the diagonal elements (ρ_{ii}) and the off-diagonal elements (σ_{ij}) of **R** can be calculated for any mixing time.

The relaxation of proton-bearing carbon-13 nuclei is dominated by the dipole−dipole interactions with neighboring protons. For carbohydrate systems, the chemical shift anisotropy is relatively small. The relaxation parameters can be expressed in terms of spectral density functions taken at different combinations of the carbon (ω_C) and proton (ω_H) Larmor frequencies. The rate for relaxation of longitudinal magnetization (R_1) is given by[33]

$$R_1 = T_1{}^{-1} = \frac{(d_{CH})^2}{4}[J(\omega_H - \omega_C) + 3J(\omega_C) + 6J(\omega_H + \omega_C)] \tag{9}$$

in which T_1 is the relaxation time of the magnetization, $d_{CH} = (\mu_0/4\pi)\gamma_H\gamma_C\hbar r_{CH}{}^{-3}$, γ_C is the magnetogyric ratio for carbons, and $r_{CH} = 1.117$ Å is the carbon−proton bond length.[34]

The reduced spectral density function, $J(\omega)$, can be described by[35]

$$J(\omega) = \frac{2}{5}\left[\frac{S^2\tau_M}{1+(\omega\tau_M)^2} + \frac{(1-S^2)\tau}{1+(\omega\tau)^2}\right] \quad (10)$$

where $\tau^{-1} = \tau_M{}^{-1} + \tau_e{}^{-1}$, τ_M is the correlation time for the global motion, common to the whole molecule, τ_e is the correlation time for internal motions, and S^2 is the square of the generalized order parameter that reflects the spatial restriction of local motion.

In the case of an axially symmetric model, the reduced spectral density function is described by[36]

$$J(\omega) = \frac{2}{5}\left(S^2\sum_{k=1,2,3} A_k\left(\frac{\tau_k}{1+(\omega\tau_k)^2}\right) + \frac{(1-S^2)\tau}{1+(\omega\tau)^2}\right) \quad (11)$$

where

$$A_1 = (1.5\cos^2\theta - 0.5)^2,\ A_2 = (3\sin^2\theta\cos^2\theta),$$
$$A_3 = 0.75\sin^4\theta,\ \tau_1 = (6D_\perp)^{-1},\ \tau_2 = (5D_\perp + D_{||})^{-1},\ \text{and}\ \tau_3 = (2D_\perp + 4D_{||})^{-1}$$

The angle between the interacting spins and the principal axis of the moment of inertia tensor is described by θ. For a symmetric top, $D_\perp = D_{xx} = D_{yy}$ and $D_{||} = D_{zz}$ with $D_{iso} = (D_{||} + 2D_\perp)/3$.

For the general case of anisotropic rotational diffusion we have[37-41]

$$J(\omega) = \frac{2}{5}\left(S^2\sum_{k=1}^{5} A_k\left(\frac{\tau_k}{1+(\omega\tau_k)^2}\right) + \frac{(1-S^2)\tau}{1+(\omega\tau)^2}\right) \quad (12)$$

with

$$\tau_1 = (4D_{xx} + D_{yy} + D_{zz})^{-1},\ \tau_2 = (D_{xx} + 4D_{yy} + D_{zz})^{-1},\ \tau_3 = (D_{xx} + D_{yy} + 4D_{zz})^{-1},\ \tau_4 = \{6D_{iso} + 6(D_{iso}{}^2 - L^2)^{1/2}\}^{-1},\ \tau_5 = \{6D_{iso} - 6(D_{iso}{}^2 - L^2)^{1/2}\}^{-1},$$
$$A_1 = 6y^2z^2,\ A_2 = 6x^2z^2,\ A_3 = 6x^2y^2,\ A_4 = d - e,\ A_5 = d + e,\ d = [3(x^4 + y^4 + z^4) - 1]/2,\ e = [\delta_x(3x^4 + 6y^2z^2 - 1) + \delta_y(3y^4 + 6x^2z^2 - 1) + \delta_z(3z^4 + 6x^2y^2 - 1)]/6,\ \delta_i = (D_{ii} - D_{iso})/(D_{iso}{}^2 - L^2)^{1/2}$$

D_{xx}, D_{yy}, and D_{zz} are the principal values of the diffusion tensor with $D_{iso} = (D_{xx} + D_{yy} + D_{zz})/3$ and $L^2 = (D_{xx}D_{yy} + D_{xx}D_{zz} + D_{yy}D_{zz})/3$. In the above, x, y, and z are the directional cosines of the interacting spins with respect to each diffusion axis.

The Stokes−Einstein expression relates the translational diffusion constant (D_t) to a sphere of radius a according to[42,43]

$$D_t = \frac{k_B T}{6\pi\eta a} \quad (13)$$

where k_B is the Boltzmann constant, T is the temperature, and η is the viscosity of the medium. The rotational correlation time (τ_r), as measured by NMR relaxation, is described by the Debye−Stokes equation[44,45]

$$\tau_r = \frac{8\pi\eta a^3}{6k_B T} = \frac{\eta V}{k_B T} \quad (14)$$

where V is the volume of a sphere.

The diffusion anisotropy can be estimated from[46]

$$D_{||}/D_\perp \approx (I_\perp/I_{||})^{1/\sqrt{2}} \quad (15)$$

where $I_\perp = (I_x + I_y)/2$, and $I_{||} = I_z$. Although this scaling overestimates the motional anisotropy somewhat,[36,46] we use it as a first approximation in the present case.

Results and Discussion

The ^{1}H and ^{13}C NMR spectra of trisaccharide **1** were assigned using 2D NMR techniques, and the chemical shifts are reported in Table 1. It can be noted that the glycosyloxylated carbons C2 and C3 have highly similar resonance frequencies, but that they still could be resolved at a magnetic field strength of 14 T. The glycosylation shifts ($\Delta\delta$) in **1** (Table 1) are similar to those of the constituent disaccharides,[47] indicating a similar conformational space at each glycosidic linkage. However, the previous study of **1** suggested that the ψ torsion angles could take only certain values (vide supra).[20]

A molecular dynamics (MD) simulation was performed on **1** with explicit water as the solvent. The conformational space sampled in the simulation is presented as ϕ/ψ scatter plots in Figure 2, and the averages for the glycosidic torsion angles are compiled in Table 2. The ϕ torsions are mainly confined to single conformational states with only limited excursions to other conformations. There is, however, some difference in the RMSDs at these torsion angles, revealing a somewhat larger flexibility at ϕ_3 compared to ϕ_2, which may simply be due to steric interactions (vide infra). The larger flexibility (large RMSD) at the ψ torsion angles as they span an extended region has been observed for this type of glycosidic torsion in oligosaccharides.[48]

For small and medium-sized oligosaccharides ^{1}H,^{1}H T-ROESY[29] or ^{1}H,^{1}H off-resonance ROESY[49] experiments are preferable to regular ^{1}H,^{1}H NOESY experiments, in which NOEs may be small as a result of an unfortunate combination of the correlation time of the molecule and the magnetic field strength of the spectrometer, i.e., the Larmor frequency of the proton nuclei in this case. In addition, the use of one-dimensional experiments may improve the quality of the data significantly, since the time spent on acquisition can be focused on a few selective excitations instead of a large number of T_1 increments.[50] Furthermore, the T-ROESY spin-lock is particularly powerful in that there is an almost complete elimination of TOCSY magnetization transfer, even when the RF transmitter is positioned in the spectral region of interest.[31] Selective excitations of resolved proton resonances were used in the ^{1}H,^{1}H T-ROESY experiments, and several Overhauser effects could be identified. Build-up curves were generated from which the proton−proton cross-relaxation rates could be extracted (Table 2). Subsequently, a reference distance was chosen from the MD simulation, viz., H1″−H2″. From an ISPA analysis, the unknown distances were calculated (Table 3). For the trans-glycosidic proton pairs stemming from the anomeric carbons of the terminal residues and those of the glycosyloxylated carbons, distances are short, ~2.25 Å. The results from the MD simulation show excellent agreement to those from the experi-

TABLE 1: Chemical Shift Assignments of ^{1}H and ^{13}C Resonances in 1[a]

residue	atom	^{1}H (ppm)	$\Delta\delta_H$[b]	^{13}C (ppm)	$\Delta\delta_C$[b]	T_1 (ms)[c]	$T_{1,fit}$ (ms)
α-L-Rha*p*-(1→3)	1″	5.06	−0.06	102.98	8.14	628 {12}	620
	2″	4.06	0.14	70.91	−0.90	665 {18}	636
	3″	3.724	−0.09	71.14	0.14	579 {11}	584
	4″	3.48	0.03	72.81	−0.38	568 {9}	588
	5″	3.708	−0.15	70.21	1.09	569 {14}	581
	6″	1.32	0.04	17.52	−0.15	nd[d]	
α-L-Rha*p*-(1→2)	1′	5.01	−0.11	102.46	7.62	651 {6}	630
	2′	4.01	0.09	71.10	−0.71	700 {21}	633
	3′	3.80	−0.01	71.00	0.00	653 {14}	650
	4′	3.46	0.01	72.88	−0.31	634 {13}	658
	5′	3.75	−0.11	70.00	0.88	634 {17}	643
	6′	1.28	0.00	17.49	−0.18	nd[d]	
→2,3)-α-L-Rha*p*-OMe[e]	1	4.80	0.11	100.34	−1.40	520 {11}	504
	2	4.005	0.08	78.26	7.32	532 {12}	539
	3	3.90	0.18	78.29	6.99	525 {12}	529
	4	3.59	0.14	72.74	−0.27	536 {12}	554
	5	3.72	0.06	69.66	0.43	541 {15}	540
	6	1.32	0.02	17.43	−0.03	nd[d]	

[a] Resonances taken at 313 K. [b] Glycosylation shifts ($\Delta\delta$) are calculated by subtraction of the chemical shifts from those of the corresponding hexose and methyl hexoside. A positive difference indicates a downfield shift. [c] Carbon-13 T_1 relaxation data recorded at 14.1 T. The 95% confidence interval is shown in braces. [d] Not determined. [e] Chemical shift of the *O*-methyl group: δ_H 3.42; δ_C 55.73.

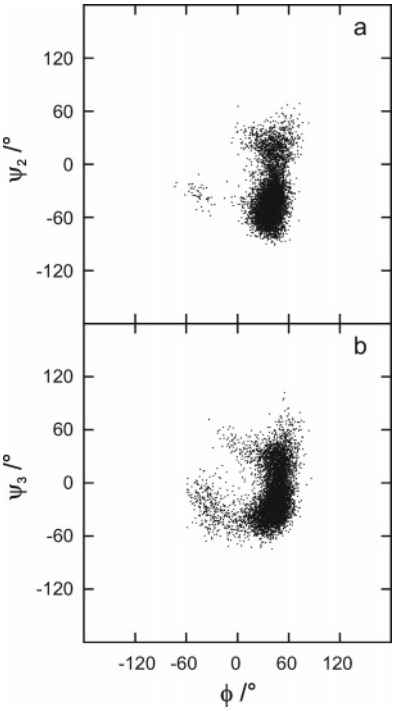

Figure 2. Scatter plots of ϕ vs ψ from the MD simulation of **1** showing the (1→2)-linkage (a) and the (1→3)-linkage (b).

TABLE 2: Glycosidic Torsion Angle (deg) Averages of 1 from MD and LD Simulations

torsion angle	MD	$^3J_{H,C}$[a] (Hz)	LD
ϕ_2	39 (13)[b]	3.9 {4.0}	37 (13)
ψ_2	−35 (29)	3.5 {nm}[c]	−40 (24)
ϕ_3	39 (20)	3.5 {3.7}	45 (11)
ψ_3	−12 (29)	5.0 {5.1}	−12 (23)

[a] Heteronuclear trans-glycosidic coupling constants were calculated from the MD simulation. Experimental $^3J_{H,C}$ values are shown in braces. [b] Root-mean-square deviations (RMSDs) are given in parentheses. [c] nm = not measured.

ment. Across the (1→2)-linkage, the distances for the H1−H1′ and H1−H5′ pairs are well described by the simulation, with only small deviations to the experimentally determined distances. The latter proton−proton distances are anti-correlated, and only a small change in the populations of the ψ_2 states (vide infra) will lead to complete agreement. The H1″−H2 interaction, for which simulated data show excellent agreement to experimental values, has a geometrical relationship across the (1→3)-linkage similar to that of the H1−H1′ at the (1→2)-linkage. Proton−proton interactions between the terminal groups were measured for the H1′−H3″ and H1′−H5″ pairs, showing a deviation in the first case but excellent agreement in the second case. Overall, the proton−proton distances derived from the simulation agree well with the effective distances derived from the T-ROESY experiments. In trisaccharide **1** there are four major degrees of freedom, each populating two conformational states. However, not all combinations are populated; some are not possible because of steric clashes, and others are only higher-energy conformers on the potential energy surface; thus their contributions may be negligible. Consequently, small changes in the potential energy function describing the trisaccharide in water may result in even better agreement. On the basis of the comparison of proton−proton distances derived from NOE data, the simulation agrees well with experimental values.

To obtain further information on conformational preferences at a glycosidic linkage, heteronuclear trans-glycosidic coupling constants are important descriptors. The $^3J_{C,H}$ values may subsequently be analyzed via a Karplus-type relationship, e.g., averaged over the potential energy surface in a Metropolis Monte Carlo simulation, or as their time dependence from an MD trajectory. We have previously been measuring the $^3J_{C,H}$ values using selective excitation of ^{13}C signals, also with the use of a Hadamard spectroscopy.[51] This technique was employed for **1**. In the resulting ^{1}H-detected spectrum, homonuclear couplings are observed in-phase and the sought heteronuclear couplings in anti-phase (Figure 3). In some cases it is possible to determine the $J_{C,H}$ value directly from the anti-phase splitting in the peak.[13] However, most often the *J*-doubling procedure is used to extract the coupling constants, because partial cancellation makes it hard to measure them directly. Through multiplication with different trial couplings (*J**), the sought-for *J* coupling can be identified (Figure 4). The experimentally derived $^3J_{C,H}$ values are shown in Table 1. One of the coupling constants was not possible to determine with this technique because of spectral overlap. As is usually the case, the $^3J_{C,H}$ values related to the ϕ torsion angles were smaller than those for the ψ torsions. Using the most recent Karplus-type relationship derived for trans-glycosidic correlations,[52] we calculate the

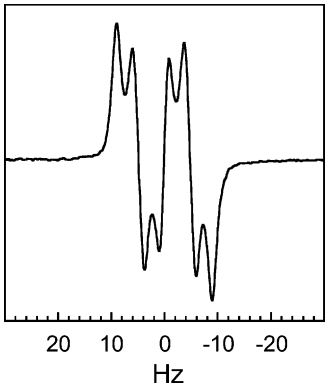

Figure 3. H3 resonance of **1** after selective excitation of the C1″ resonance to detect the trans-glycosidic $^3J_{H,C}$ coupling.

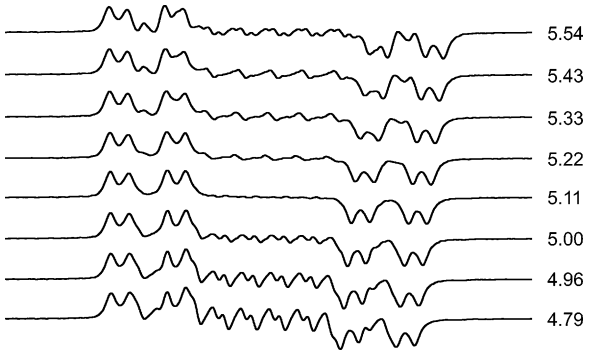

Figure 4. Application of the *J*-doubling procedure facilitates determination of the experimental $^3J_{H,C}$ value in **1** between C1″ and H3 because when the trial coupling constant $J^* = J$, the integral has its minimum (5.1 Hz) and the in-phase *dd* pattern is retained.

$^3J_{C,H}$ values from the MD trajectory. The agreement to experimental data is excellent for the three measured coupling constants. Thus, in this respect the simulation describes the conformational dynamics of the trisaccharide. It should be further noted that the precision in the determination of the $^3J_{C,H}$ values is very high, on the order of ±0.1 Hz.[53−55] Therefore the difference in $^3J_{C,H}$ values related to the ϕ torsion angles, 4.0 vs 3.7 Hz, indicates a change in population averaging at the two torsion angles (vide infra).

As noted in the Introduction, stereochemical arrangements in **1** are similar to the branching region (α-L-Rha*p*-(1→2)[*β*-D-Glc*p*NAc-(1→3)]-α-L-Rha*p*) in the cell-wall polysaccharide from *Streptococcus* group A. Because different oligosaccharides are compared, the structural comparison should not be taken too far, but of the comparable structures (as a result of similar stereochemical arrangements), four out of five proton−proton interactions are very similar in a pentasaccharide containing the branching region.[18] The study of oligosaccharides related to the polysaccharide from *Streptococcus* group A utilized three force fields to sample the conformational space, all different from that used herein, and consequently the resulting scatter plots were different, as well.

In an analysis of the conformation and dynamics of molecules, it may be suitable to describe systems in terms of conformational states, their relative proportions, and the transitions between energy wells. As noted above, in the previous study of **1** two conformers of low potential energy were identified after energy minimization. The time dependence of the four glycosidic torsion angles between the sugar residues in **1** is shown in Figure 5. Besides their usual exoanomeric conformation, the ϕ torsions make transitions to a non-exoanomeric conformation. At the (1→3)-linkage these transitions occur several times during the

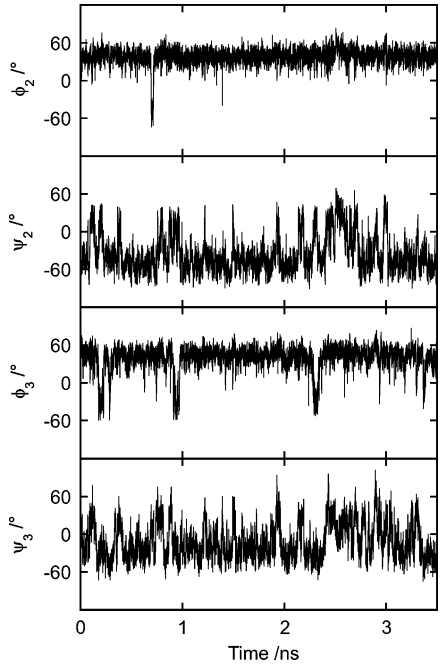

Figure 5. Time dependence from the MD simulation of **1** showing the glycosidic torsion angles.

simulation, indicating that this conformational state is indeed populated to a small but still significant degree. Because **1** is a vicinally disubstituted trisaccharide, transitions at the various torsions may or may not be correlated to each other. It is indicated that the transitions at ϕ_3 can occur quite independently with respect to the other torsions. For ϕ_2, only a single transition occurs to the non-exoanomeric conformation, in which its occupancy lasts only for a limited time. The ψ torsion angles indeed fluctuate a great deal (RMSD = 29°). For each of the torsions, this may be described as a ψ^+ or a ψ^- conformational state. However, transitions are rapid, and no well-defined state lasting for a relatively long time is apparent, such as for α-D-Man*p*-(1→2)-α-D-Man*p*-(1→*O*)-L-Ser, in which hydrogen bonding between the hydroxymethyl groups was present when a well-defined conformation of low fluctuations (RMSD = 8°) existed.[56] In **1** such hydrogen bonding is of course not possible, because at all C6 positions there are methyl groups.

The water structure around a methyl group is also quite different,[57] leading to an altered environment with different interactions at the (1→2)-linkage of **1** for the ψ^- conformational state, corresponding to the ψ^+ conformational state of the mannosyl-containing disaccharide. Inspection of the time dependence of the ψ torsion angles, although highly flexible, indicates that transitions are correlated (Figure 5). Thus, we have analyzed the time dependence of the ψ torsion angles to investigate the degree of correlation between the conformational states. In dividing the conformational states by the crossing at 0° (close to the saddle point of this type of linkages)[13,25] into ψ^+ and ψ^-, one obtains the following populations: $\psi_2{}^+ = 0.15$, $\psi_2{}^- = 0.85$, $\psi_3{}^+ = 0.31$, and $\psi_3{}^- = 0.69$. We may then ask the following question: To what extent are the two positive and two negative states correlated? This was analyzed by identification of different states, namely, $\psi_2{}^+\psi_3{}^+$ and $\psi_2{}^-\psi_3{}^-$, both of which then correspond to a value of unity, whereas the other combinations, $\psi_2{}^+\psi_3{}^-$ and $\psi_2{}^-\psi_3{}^+$, are labeled by a value of zero. The population of the former combinations is thus a measure of the degree of correlation, and was found to be 0.77

TABLE 3: Cross-Relaxation Rates σ and Proton−Proton Distances r for Trisaccharide 1 Derived from 1D ^{1}H,^{1}H T-ROESY NMR Experiments Using ISPA and from the MD Simulation

proton pair	σ (s^{-1})	r_{exp} (Å)	r_{MD}[a] (Å)
H1″−H2″	0.070	2.54[b]	2.54
H1″−H3	0.148	2.24	2.26
H1″−H2	0.016	3.24	3.20
H1′−H2	0.14	2.25	2.29
H1′−H3″	0.043	2.76	3.47
H1′−H5″	0.052	2.67	2.67
H1−H1′	0.019	3.16	2.84
H1−H5′	0.075	2.51	2.73

[a] $1/r = \langle r^{-6}\rangle^{1/6}$ from simulation. [b] Reference distance from MD simulation.

TABLE 4: Effective Proton−Proton Distances r[a] for Different Conformational States Populated by Trisaccharide 1 from the LD Simulation

proton pair	ψ^+ [b]	ψ^- [c]	ϕ_2 (non-exo)[d]	ϕ_3 (non-exo)[e]
H1″−H2″	2.53	2.52	2.52	2.54
H1″−H3	2.67	2.22	2.48	2.24
H1″−H2	4.40	3.48	4.27	2.53
H1′−H2	2.28	2.29	2.33	2.26
H1′−H3″	2.45	4.75	5.01	5.11
H1′−H5″	2.57	2.61	3.96	3.19
H1−H1′	4.01	2.70	2.37	3.85
H1−H5′	2.40	3.02	4.44	2.47

[a] Averaged as $1/r = \langle r^{-6)1/6}$ [b] $\langle\phi_2\rangle = 40°$, $\langle\psi_2\rangle = 13°$, $\langle\phi_3\rangle = 55°$, $\langle\psi_3\rangle = 32°$. [c] $\langle\phi_2\rangle = 35°$, $\langle\psi_2\rangle = -50°$, $\langle\phi_3\rangle = 47°$, $\langle\psi_3\rangle = -22°$. [d] $\langle\phi_2\rangle = -30°$, $\langle\psi_2\rangle = -28°$, $\langle\phi_3\rangle = 45°$, $\langle\psi_3\rangle = 25°$. [e] $\langle\phi_2\rangle = 39°$, $\langle\psi_2\rangle = 1°$, $\langle\phi_3\rangle = -22°$, $\langle\psi_3\rangle = -26°$.

from the MD simulation. Therefore, although these torsions are highly flexible, correlated motions are observed for the ψ torsion angles.

The discrepancy in the effective H1′−H3″ distance between experiment and simulation prompted further analysis of the trisaccharide. We first note that an increase in the population of the ψ_2^+ state will lead to a better agreement between the effective distances in the MD simulation and those derived from the NMR T-ROESY experiment for both the H1−H1′ and H1−H5′ pairs. Unfortunately, the $^3J_{C,H}$ coupling constant related to the ψ_2 torsion angle was not possible to extract with any confidence, which could have indicated a significant deviation for the simulation. With a larger population of the ψ_2^+ state and consequently the ψ_3^+ state, as these are highly correlated, the effective H1′−H3″ distance will be shorter, thereby resolving this part of the comparison between experiment and simulation.

In the following analysis we utilize a Langevin dynamics (LD) simulation, which showed conformational properties similar to that of the MD simulation (Table 2). From the LD simulation four conformational states were identified (Table 4), related to either ψ torsion angles or non-exoanomeric conformations, as previously indicated by the MD trajectories (Figure 5). It should be noted that the extent of population of the ϕ_2 non-exoanomeric conformational state is higher in the MD simulation containing explicit water molecules than in the LD simulation. After averaging of each conformational state present in the simulation, effective distances were obtained. Short distances are quite insensitive to the presence of other conformational states because of the r^{-6} averaging of the nuclear Overhauser effect. To obtain the relative population ratio of multiconformer structures from NMR NOE-based approaches, high-quality quantitative data are a prerequisite.[58] Least-squares fitting of the inter-residue distances (except for H1′−H2, which is short and insensitive) for the four conformational states to the experimentally derived distances resulted in populations of 0.48, 0.36, 0.00, and 0.16 for the $\psi_2^+\psi_3^+$, $\psi_2^-\psi_3^-$, ϕ_2 (non-exo), and ϕ_3 (non-exo) states, respectively. Thus, the two major conformational states identified above are present in roughly equal amounts. Notably, of the non-exoanomeric ϕ conformational states, that of ϕ_3 is indeed populated to a significant degree. From a simulation (and force field) point of view, it is very convincing that the minor states identified in the MD simulation (Figure 5) are indeed correctly determined in the sense that ϕ_3 is populated to a low but significant extent. The ϕ_2 torsion angle is hardly present at all in either the simulation or the analysis based primarily on the experimental NMR data. Recently, the presence of a non-exoanomeric ϕ conformational state (∼20−30%) was detected at the ribofuranosyl residue in the oligosaccharide neomycin-B.[59,60] For the hexopyranosyl rhamnose residue investigated herein, the ϕ_3 (non-exo) state is populated to a lower extent as part of a conformational equilibrium with other states, in a manner similar to that observed for the α-mannopyranosyl residue in a trehalose-like system.[61]

To further investigate the dynamics of the trisaccharide, we now turn to additional NMR techniques, namely, the longitudinal eddy-delayed experiment for the determination of the translational diffusion constant, and carbon-13 T_1 relaxation measurements, which were performed at 14.1 T, where all ring carbons were resolved. The spin−lattice relaxation times were observed in the range 520−700 ms (Table 1). The translational diffusion coefficient $D_t = 3.2 \times 10^{-10}$ m^2/s at 25 °C. Employing the Stokes relationships (eqs 13 and 14) and a correction factor[62] of 1.12, as the sample is not at infinite dilution, as well as the correction for the higher viscosity of D_2O compared to H_2O, we obtain a rotational correlation time $\tau_r = 150$ ps at 40 °C. Internal dynamics can be described by the Lipari−Szabo type order parameter denoted S^2,[35] which for a rigid molecular fragment is unity, and becomes zero for completely unrestricted motion. The ^{13}C T_1 relaxation times can be calculated using eqs 9 and 10. If the trisaccharide tumbles as a rigid entity, the observed values of T_1 should be <500 ms, which is not the case. Thus, from the ^{13}C T_1 data, internal dynamics are present, and S^2 for each sugar residue is less than unity. Assuming an isotropic rotational diffusion model and $\tau_e = 10$ ps, one can estimate $S^2 \approx 0.9$ for the disubstituted rhamnosyl residue, and $S^2 \approx 0.7$ for the two terminal sugar residues. This is in good agreement with those previously determined by multiple-field ^{13}C relaxation studies on similar trisaccharides.[63] It is evident that the T_1 values differ not only between the sugar residues but also within a residue. The differences between the residues are most readily interpreted as different dynamics for each sugar in the trisaccharide. However, since the rhamnosyl residues in trisaccharide **1** have the pyranoid ring form, only limited internal ring motion is anticipated for each residue per se. Furthermore, in α-Rha*p* residues the C1−H1, C2−H2, and C3−H3 bond vectors are roughly orthogonal to each other in the ring coordinate system, whereas those for C3−H3, C4−H4, and C5−H5 are essentially parallel. Thus, we have probes that can reveal information also on nonisotropic rotational motion. For the disubstituted *O*-methyl residue, the ^{13}C T_1 values are very similar, with an average of ∼530 ms. These values are consistent with $S^2 \approx 0.86$, and are not particularly sensitive to the conformation of **1** when a nonisotropic model is used. However, in the primed residue that is (1→2)-linked, the T_1 values of C2 ≠ C1 ≈ C3−C5, whereas in the doubly primed residue that is (1→3)-linked, T_1 of C1 ≠ C2 ≠ C3−C5. These data indicate that a model of higher complexity is needed.

The anisotropy is not large for the trisaccharide having the relative principal components of the moment of inertia tensor I_{xx}:I_{yy}:I_{zz} as ~2:1.5:1.0, but even after scaling (cf. eq 15) on the basis of hydrodynamic considerations, the description still differs from a symmetric top. Least-squares fitting of S^2 to the ^{13}C T_1 relaxation data for each sugar ring of a dynamically population averaged anisotropic rotational model, using a mean C−H bond distance of 1.117 Å,[32] resulted in $S^2 = 0.74$ for the double primed ring of the (1→3)-linked residue, $S^2 = 0.70$ for the primed ring of the (1→2)-linked residue, and $S^2 = 0.86$ for the nonprimed ring of the disubstituted residue. Good agreement with experimental data is observed (Table 1), except for C2′, which showed the largest uncertainty in the T_1 determination (Table 1). Taking into account the ^{13}C T_1 relaxation data, in addition to the ^{1}H,^{1}H T-ROE data, in the least-squares fitting to the four conformational states, we obtained the populations 0.49, 0.39, 0.00, and 0.12 for the $\psi_2^+\psi_3^+$, $\psi_2^-\psi_3^-$, ϕ_2 (non-exo), and ϕ_3 (non-exo) states, respectively.

The use of the inertia tensor (scaled) in lieu of the diffusion tensor has recently been shown to be an excellent approximation for oligosaccharides.[64] Least-squares fitting to the ^{13}C T_1 relaxation data for the individual resonances resulted in slightly lower S^2 values for, in particular, C2″ and C2′ compared to the other carbon atoms in the respective sugar residue, indicative of some additional dynamics (anisotropy of internal motion). This was further investigated by calculation of S^2 for the three populated conformational states as the plateau of the reorientational correlation function $\langle P_2(\mu(0)\,\mu(t))\rangle$, in which the overall rotation has been removed.[35,36] The S^2 values for the C−H pairs of the disubstituted *O*-methyl residue were generally ≥0.9, whereas for the primed and the double primed rings they were ≤0.9, consistent with different flexibility as deduced from the ^{13}C T_1 relaxation data. Although some differences were observed for the C−H pairs, a significant deviation was not present for the C2′−H2′ pair, which has the longest T_1 value, or for the C2″−H2″ pair. Analysis of the proton−proton interactions revealed different S^2 values in the three states, further revealing the complexity of this system.

Selected ^{1}H,^{1}H T-ROE buildup curves determined from the experiment are shown in Figure 6a. From the derived model in which the trisaccharide is described as a dynamically interconverting anisotropically tumbling system, we calculate ^{1}H,^{1}H T-ROE buildup curves using a full-relaxation matrix approach for selected inter-residue correlations (Figure 6b). The S^2 values for the interacting proton pairs are not known, but to a first approximation we use the average of the pertinent sugar rings, giving $S_{HH}^2 = 0.80$ for H1″−H3, $S_{HH}^2 = 0.74$ for H1″−H2″, and $S_{HH}^2 = 0.72$ for H1′−H3″. The T-ROE buildup curves show excellent agreement for the intraring reference distance H1″−H2″ as well as the interaction between the two terminal rhamnosyl residues as analyzed by the H1′−H3″ T-ROE. For the H1″−H3 interaction, the calculated curve is slightly lower. However, comparison to the experimentally determined effective distance, when excitations from both resonances are averaged (Table 3), shows that it differs by only 4%. We also note that to reproduce the ^{1}H,^{1}H cross-relaxation buildup curves, the use of an isotropically reorienting system is sufficient in this case (data not shown).

In conclusion, the conformational analysis of α-L-Rha*p*-(1→2)[α-L-Rha*p*-(1→3)]-α-L-Rha*p*-OMe in a water solution revealed a highly flexible system. In contrast to the previous study, which proposed a dominant $\psi_2^-\psi_3^-$ conformational state for the trisaccharide as determined from simple force field calculations and steady-state ^{1}H,^{1}H NOE experiments, we herein identify a conformational equilibrium of interconverting states between not only $\psi_2^+\psi_3^+$ and $\psi_2^-\psi_3^-$ as the major states but also the ϕ_3 (non-exo) state (Figure 7). The conformational flexibility within the potential energy wells was evident from the ^{13}C T_1 NMR relaxation measurements, which also indicated some anisotropic motion(s) of the molecule. With the aid of

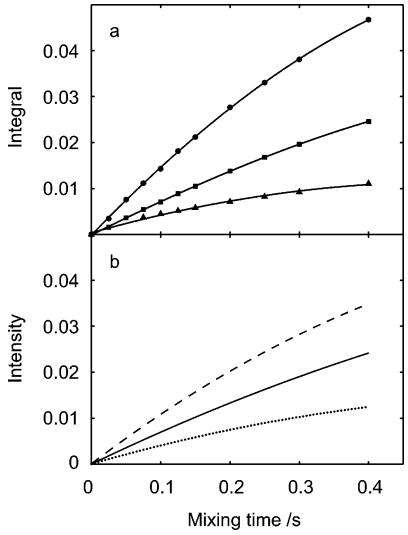

Figure 6. ^{1}H,^{1}H T-ROESY NMR buildup curves. (a) Excitation of anomeric resonances resulting in cross-relaxation between the transglycosidic protons H1″−H3 (●) ($\sigma = 0.159$ s^{-1}), the proton pair H1″−H2″ (■) ($\sigma = 0.077$ s^{-1}) used as a reference distance, and the H1′−H3″ protons (▲) ($\sigma = 0.043$ s^{-1}) between adjacent rhamnosyl groups in **1**. (b) Simulation based on the full relaxation matrix approach, assuming equal weights of the longitudinal and transverse autorelaxation rate constants, for a dynamic and population-averaged anisotropically reorienting molecule: the H1″−H3 pair (solid line) ($\sigma = 0.114$ s^{-1}), H1″−H2″ (dashed line) ($\sigma = 0.072$ s^{-1}), and H1′−H3″ (dotted line) ($\sigma = 0.043$ s^{-1}) in the trisaccharide.

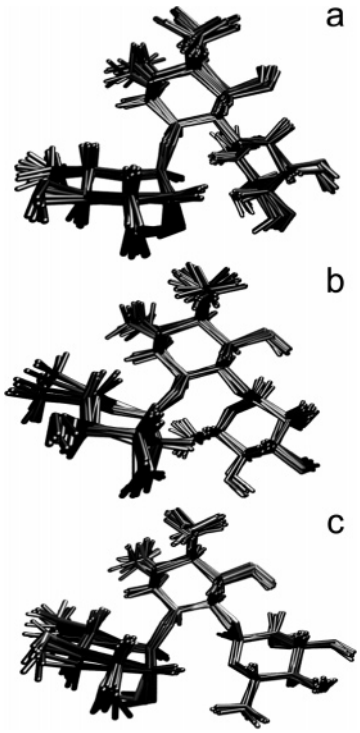

Figure 7. Molecular model with 10 structures from the LD simulation of the trisaccharide, in which the overlay is based on the average structure for each of the three populated conformational states: ψ_2^+ ψ_3^+ (a), ψ_2^- ψ_3^- (b), and ϕ_3 (non-exo) (c).

computer simulations in conjunction with NMR spectroscopy, we were able to identify conformational families and generate a dynamic and population-averaged model from which we could calculate ^{1}H,^{1}H T-ROE buildup curves that were in very good agreement with those obtained from the experiment. The complex conformational preferences and the dynamics of medium-sized molecules such as oligosaccharides[65,66] and peptides[67] are thus becoming clearer. These results form the basis of future interaction studies between, for example, carbohydrate ligands and their binding to proteins,[68] because from a pool of different conformations one or a few can be selected or bound in an induced-fit manner.[69]

Materials and Methods

General. The synthesis of **1**, described briefly, was performed by glycosylation of methyl 4-*O*-benzyl-α-L-rhamnopyranoside with 2,3,4-tri-*O*-benzoyl-α-L-rhamnopyranosyl bromide, using silver triflate as a promoter. Subsequent workup followed by deprotection of the bensyl and benzoyl groups under standard conditions and purification by gel permeation chromatography yielded the trisaccharide. Chemical shift assignments of its ^{1}H and ^{13}C NMR resonances were performed by 2D NMR techniques, and showed very good agreement to those published,[20] thereby confirming the identity of the synthesized product. The chemical shifts were compared to those of the corresponding hexose and methyl hexoside.[19,70]

The atoms of the terminal (1→3)-linked residue are designated with a double prime; those in the terminal (1→2)-linked residue are designated with a prime, and those in the *O*-methyl rhamnoside are unprimed. The torsion angles across the glycosidic linkages are defined as ϕ_2 = H1′−C1′−O2−C2, ψ_2 = C1′−O2−C2−H2, ϕ_3 = H1″−C1″−O3−C3, and ψ_3 = C1″−O3−C3−H3. The conformational state for which both ψ torsion angles show positive values is denoted by $\psi_2^+\psi_3^+$, and consequently the $\psi_2^-\psi_3^-$ state has negative torsion angles. Calculations of NMR observables, such as ^{13}C T_1 relaxation times, ^{1}H,^{1}H T-ROE buildup curves, effective distances, and related entities from the MD and LD simulations, were performed with a MATLAB-based program called SIMMA (SIMulation and Molecular Analysis) implemented to this end.

NMR Spectroscopy. The trisaccharide was treated with CHELEX 100 in order to remove any paramagnetic ions. The sample was freeze-dried and dissolved in 0.7 mL of D_2O to give a total concentration of 100 mM, transferred to a 5 mm NMR tube, and flame-sealed under vacuum after degassing by three freeze−pump−thaw cycles. All NMR experiments were performed on a Varian INOVA 600 spectrometer at 313 K.

Proton−proton cross-relaxation rates (σ) were measured with one-dimensional DPFGSE T-ROESY experiments.[31,71] Selective excitations were enabled using 25−15 Hz broad i-Snob-2 shaped pulses[72] of 68−113 ms duration. The gradient durations in the initial DPFGSE part were 1 ms and the strengths 0.8 and 2.3 G cm^{-1}. The DPFGSE part was followed by a T-ROESY spin-lock with $\gamma B_1/2\pi$ = 2.5 kHz. Spectra were recorded using a width of 1200 Hz and 4800 complex points. For each mixing time, 944 transients were used. The total relaxation delay between the transients was 10 s, which corresponds to $>5T_1$. Ten different ^{1}H,^{1}H cross-relaxation delays (mixing times) between 50 and 800 ms were used. Prior to Fourier transformation, the FIDs were zero-filled and multiplied with a 1 Hz exponential line-broadening factor. Spectra were phased, drift corrected, and baseline corrected using a first-order correction, and integrated using the same integration limits at all mixing times.

Integrated auto-peaks were fitted to an exponentially decaying function. The integrals from cross-relaxation peaks were normalized by division of the extrapolated auto-peak values at zero mixing time. Cross-relaxation buildup curves were obtained from the normalized integrals at different mixing times, and the rates were calculated by fitting to a second-order polynomial up to 400 ms. The least-squares fits, expressed using the regression coefficient, showed $R > 0.98$ in all cases. When possible, each distance reported in Table 2 is an average of the two cross-relaxation rates obtained from excitations at the different proton resonance frequencies of a proton pair, e.g., from H1″ to H3 and vice versa.

Measurements of the trans-glycosidic carbon−proton coupling constants were performed as a single ^{13}C site-selective excitation as well as a Hadamard-2 excitation using a 50 ms half-Gaussian shaped pulse[73] with a pulsed field gradient version of the pulse sequence.[74] The delay for evolution of the heteronuclear couplings was set to 30 ms, and the spectral range was 1400 Hz. The FID was sampled with 5632 complex data points, and the number of transients was 10 880. Eight times zero-filling and multiplication of the FID with a 0.3 Hz exponential broadening factor were applied prior to Fourier transformation. Coupling constants were extracted by the *J*-doubling procedure, using eight delta functions in the frequency domain.

Carbon-13 T_1 relaxation measurements were performed at 14.1 T with a broadband probe. The fast inversion−recovery method[75] was used with a nonlinear fit of line intensities. Eight different relaxation delay times (10 ms to 1.2 s) were sampled with 2048 scans at each delay. The prescan delay was set to 1.2 s. The spectral width was 8000 Hz covering the ring carbons, and 12 800 complex data points were sampled. The FIDs were zero-filled to 32K data points and multiplied with a 1 Hz exponential line-broadening factor prior to Fourier transformation. Relaxation data are averages of eight independent measurements taken without removing the sample from the spectrometer.

Translational diffusion measurements were performed at 298 K. The deviation from linearity of the pulsed-field-gradient (PFG) pulses over the sample volume was characterized as described by Damberg et al.[76] The Stejskal−Tanner spin−echo experiment[77] with an additional gradient pre-pulse, which purges all transverse magnetization from the previous FID and makes the two diffusion encoding gradient pulses more equal, was followed by an additional weak gradient during the acquisition period, which enables spatial resolution along the *z*-axis. The distribution of the gradient strengths was modeled by a simple truncated linear gradient, resulting in calibrated conditions for a sample with a known translational diffusion coefficient (1% H_2O in D_2O + 1 mg/mL $GdCl_3$; $D_t = 1.90 \times 10^{-9}$ m^2 s^{-1} at 298 K).[78] The gradient strengths were varied between 0.5 and 14.6 G cm^{-1} in 30 steps. The duration of the PFG pulses was 5 ms, and the refocusing delay was 50 ms. Diffusion coefficients of the trisaccharide were obtained by the longitudinal eddy-delayed experiment.[79] The gradient strengths were in the range 0.5−8.8 G cm^{-1}. The duration of the PFG pulses was 5 ms, and the refocusing delay was 100 ms. In addition, dephasing gradients were applied after the second and fourth 90° pulses as well as after the acquisition period. Subsequently, a nonlinear two-parameter fit (A_0 and D_t) of the attenuation of signal intensities was performed.

Molecular Simulations. Molecular dynamics (MD) simulations used CHARMM[80] (parallel version, C27b4) employing a CHARMM22 type of force field,[81] namely PARM22/SU01,[82] which is a recently modified force field for carbohydrates. Initial

conditions were prepared by placing trisaccharide **1** in a previously equilibrated cubic water box of length 29.97 Å containing 900 TIP3P water[83] molecules, and by removing the solvent molecules that were closer than 2.5 Å to any solute atom. This procedure resulted in a system with the trisaccharide and 871 water molecules. Energy minimization was performed with Steepest Descent, 200 steps, followed by Adopted Basis Newton−Raphson until the root-mean-square gradient was less than 0.01 kcal mol^{-1} $Å^{-1}$. The MD simulation was carried out with the leapfrog algorithm,[84] a time step of 1 fs, and a dielectric constant of unity. Initial velocities were assigned at 103 K followed by heating at 5 K increments during 8 ps to 313 K, at which point the system was equilibrated for 200 ps. The production run having a 3.5 ns duration was temperature-scaled around 313 K by Berendsen's weak coupling algorithm.[85] Data were saved every 100 time steps for analysis. Periodic boundary conditions and the minimum image convention were used together with a heuristic nonbond frequency update and a force shift cutoff[86] acting to 12 Å. Simulations were performed on an IBM SP2 computer at the Center for Parallel Computers, KTH, Stockholm, using 16 nodes, which resulted in a CPU time of approximately 40 h ns^{-1}.

LD simulations were carried out for 18 ns at 300 K using a collision frequency $\gamma = 50$ ps^{-1} for carbon and oxygen atoms and a dielectric constant of 3. In conformational averaging of different states, 100−2000 structures were used in the analysis. For calculation of S^2, the average structure of each state (Table 4) was chosen as the reference system, and overall rotation was removed by RMS fitting of each trajectory frame to this structure. Subsequently, the correlation function was calculated from the oriented trajectory, and the S^2 value was obtained from the long time decay.

Acknowledgment. This work was supported by grants from the Swedish Research Council (VR) and Swedish National Infrastructure for Computing (SNIC).

References and Notes

(1) Yang, R.-Y.; Hsu, D. K.; Yu, L.; Ni, J.; Liu, F.-T. *J. Biol. Chem.* **2001**, *276*, 20252−20260.
(2) Matsuura, K.; Kitakouji, H.; Sawada, N.; Ishida, H.; Kiso, M.; Kitajima, K.; Kobayashi, K. *J. Am. Chem.* Soc. **2000**, *122*, 7406−7407.
(3) Woodworth, A.; Fiete, D.; Baenziger, J. U. *J. Biol. Chem.* **2002**, *277*, 50941−50947.
(4) Rundlöf, T.; Kjellberg, A.; Damberg, C.; Nishida, T.; Widmalm, G. *Magn. Reson. Chem.* **1998**, *36*, 839−847.
(5) Landersjö, C.; Stenutz, R.; Widmalm, G. *J. Am. Chem. Soc.* **1997**, *119*, 8695−8698.
(6) Ivarsson, I.; Sandström, C.; Sandström, A.; Kenne, L. *J. Chem. Soc., Perkin Trans. 2* **2000**, 2147−2152.
(7) Sheng, S.; van Halbeek, H. *Biochem. Biophys. Res. Commun.* **1995**, *215*, 504−510.
(8) Lycknert, K.; Maliniak, A.; Widmalm, G. *J. Phys. Chem. A* **2001**, *105*, 5119−5122.
(9) Freedberg, D. A. *J. Am. Chem. Soc.* **2002**, *124*, 2358−2362.
(10) Berthault, P.; Jeannerat, D.; Camerel, F.; Salgado, F. A.; Boulard, Y.; Gabriel, J.-C. P.; Desvaux, H. *Carbohydr. Res.* **2003**, *338*, 1771−1785.
(11) Söderman, P.; Jansson, P.-E.; Widmalm, G. *J. Chem. Soc., Perkin Trans. 2* **1998**, 639−648.
(12) Dixon, A. M.; Venable, R. M.; Widmalm, G.; Bull, T. E.; Pastor, R. W. *Biopolymers* **2003**, *69*, 448−460.
(13) Hardy, B. J.; Bystricky, S.; Kovac, P.; Widmalm, G. *Biopolymers* **1997**, *41*, 83−96.
(14) Jansson, P.-E.; Kenne, L.; Wehler, T. *Carbohydr. Res.* **1987**, *166*, 271−282.
(15) Dmitriev, B. A.; Knirel, Y. A.; Kochetkov, N. K.; Hofman, I. L. *Eur. J. Biochem.* **1976**, *66*, 559−566.
(16) Ansaruzzaman, M.; Albert, M. J.; Holme, T.; Jansson, P.-E.; Rahman, M. M.; Widmalm, G. *Eur. J. Biochem.* **1996**, *237*, 786−791.
(17) Kreis, U. C.; Varma, V.; Pinto, B. M. *Int. J. Biol. Macromol.* **1995**, *17*, 117−130.
(18) Höög, C.; Rotondo, A.; Johnston, B. D.; Pinto, B. M. *Carbohydr. Res.* **2002**, *337*, 2023−2036.
(19) Jansson, P.-E.; Kenne, L.; Widmalm, G. *Carbohydr. Res.* **1989**, *188*, 169−191.
(20) Lipkind, G. M.; Nifant'ev, N. E.; Shashkov, A. S.; Kochetkov, N. K. *Can. J. Chem.* **1990**, *68*, 1238−1250.
(21) Keepers, J. W.; James, T. L. *J. Magn. Reson.* **1984**, *57*, 404−426.
(22) Thomas, P. D.; Basus, V. J.; James, T. L. *Proc. Natl. Acad. Sci. U.S.A.* **1991**, *88*, 1237−1241.
(23) Baleja, J. D.; Moult, J.; Sykes, B. D. *J. Magn. Reson.* **1990**, *87*, 375−384.
(24) Post, C. B.; Meadows, R. P.; Gorenstein, D. G. *J. Am. Chem. Soc.* **1990**, *112*, 6796−6803.
(25) Widmalm, G.; Byrd, R. A.; Egan, W. *Carbohydr. Res.* **1992**, *229*, 195−211.
(26) Neuhaus, D.; Williamson, M. *The Nuclear Overhauser Effect in Structural and Conformational Analysis*; VCH: New York, 1989.
(27) Bothner-By, A. A.; Stephens, R. L.; Lee, J.-m.; Warren, C. D.; Jeanloz, R. W. *J. Am. Chem. Soc.* **1984**, *106*, 811−813.
(28) Bull, T. E. *Prog. NMR Spectrosc.* **1992**, *24*, 377−410.
(29) Hwang, T.-L.; Shaka, A. J. *J. Am. Chem. Soc.* **1992**, *114*, 3157−3159.
(30) Hwang, T.-L.; Shaka, A. J. *Magn. Reson. Chem.* **1992**, *30*, S24−S34.
(31) Hwang, T.-L.; Shaka, A. J. *J. Magn. Reson. B* **1993**, *102*, 155−165.
(32) Gentle, J. E. In *Numerical Linear Algebra for Applications in Statistics*; Springer-Verlag: Berlin, 1998; pp 93−95.
(33) Doddrell, D.; Glushko, V.; Allerhand, A. *J. Chem. Phys.* **1972**, *56*, 3683−3689.
(34) Ottiger, M.; Bax, A. *J. Am. Chem. Soc.* **1998**, *120*, 12334−12341.
(35) Lipari, G.; Szabo, A. *J. Am. Chem. Soc.* **1982**, *104*, 4546−4559.
(36) Rundlöf, T.; Venable, R. M.; Pastor, R. W.; Kowalewski, J.; Widmalm, G. *J. Am. Chem. Soc.* **1999**, *121*, 11847−11854.
(37) Woessner, D. E. *J. Chem. Phys.* **1962**, *37*, 647−654.
(38) Berger, S.; Kreissl, F. R.; Grant, D. M.; Roberts, J. D. *J. Am. Chem. Soc.* **1975**, *97*, 1805−1808.
(39) Tjandra, N.; Feller, S. E.; Pastor, R. W.; Bax, A. *J. Am. Chem. Soc.* **1995**, *117*, 12562−12566.
(40) Lee, L. K.; Rance, M.; Chazin, W. J.; Palmer, A. G., III. *J. Biomol. NMR* **1997**, *9*, 287−298.
(41) Boisbouvier, J.; Wu, Z.; Ono, A.; Kainosho, M.; Bax, A. *J. Biomol. NMR* **2003**, *27*, 133−142.
(42) Einstein, A. *Investigations on the Theory of the Brownian Movement*; Dover Publications: New York, 1956; p 58.
(43) Edward, J. T. *J. Chem. Educ.* **1970**, *47*, 261−270.
(44) Debye, P. *Polar Molecules*; Dover Publications: New York, 1929; pp 84−85.
(45) Bloomfield, V. A. Survey of Biomolecular Hydrodynamics. In *Biophysics Textbook On-line: Separations and Hydrodynamics*; Schuster, T. M., Ed.; 2000; pp 1−16.
(46) Copié, V.; Tomita, Y.; Akiyama, S. K.; Aota, S.-I.; Yamada, K. M.; Venable, R. M.; Pastor, R. W.; Krueger, S.; Torchia, D. A. *J. Mol. Biol.* **1998**, *277*, 663−682.
(47) Jansson, P.-E.; Kenne, L.; Widmalm, G. *Acta Chem. Scand.* **1991**, *45*, 517−522.
(48) Sayers, E. W.; Prestegard, J. H. *Biophys. J.* **2000**, *79*, 3313−3329.
(49) Desvaux, H.; Goldman, M. *Mol. Phys.* **1994**, *81*, 955−974.
(50) Dixon, A. M.; Widmalm, G.; Bull, T. E. *J. Magn. Reson.* **2000**, *147*, 266−272.
(51) Kupèe, E.; Nishida, T.; Freeman, R. *Prog. NMR Spectrosc.* **2003**, *42*, 95−122.
(52) Cloran, F.; Carmichael, I.; Serianni, A. S. *J. Am. Chem. Soc.* **1999**, *121*, 9843−9851.
(53) del Río-Portilla, F.; Blechta, V.; Freeman, R. *J. Magn. Reson.* **1994**, *111*, 132−135.
(54) Garza-García, A.; Ponzanelli-Velázquez, G.; del Río-Portilla, F. *J. Magn. Reson.* **2001**, *148*, 214−219.
(55) Jansson, J. L. M.; Maliniak, A.; Widmalm, G. In *Computational Chemistry of Carbohydrates*; Vliegenthart, J. F. G., Woods, R., Eds.; ACS Symposium Series; American Chemical Society: Washington, DC, 2005, in press.
(56) Lycknert, K.; Helander, A.; Oscarson, S.; Kenne, L.; Widmalm, G. *Carbohydr. Res.* **2004**, *339*, 1331−1338.
(57) Rossky, P.; Karplus, M. *J. Am. Chem. Soc.* **1979**, *101*, 1913−1937.
(58) Bonvin, A. M. J. J.; Brünger, A. T. *J. Biomol. NMR* **1996**, *7*, 72−76.
(59) Asensio, J. L.; Hidalgo, A.; Cuesta, I.; Gonzalez, C.; Cañada, J.; Vicent, C.; Chiara, J. L.; Cuevas, G.; Jimenez-Barbero, J. *Chem. Commun.* **2002**, 2232−2233.
(60) Asensio, J. L.; Hidalgo, A.; Cuesta, I.; González, C.; Cañada, J.; Vicent, C.; Chiara, J. L.; Cuevas, G.; Jimenez-Barbero, J. *Chem.—Eur. J.* **2002**, *8*, 5228−5240.

(61) Asensio, J. L.; Cañada, F. J.; Cheng, X.; Khan, N.; Mootoo, D. R.; Jiménez-Barbero, J. *Chem.—Eur. J.* **2000**, *6*, 1035−1041.
(62) Chirfe, J.; Buera, M. P. *J. Food Eng.* **1997**, *33*, 221−226.
(63) Kjellberg, A.; Rundlöf, T.; Kowalewski, J.; Widmalm, G. *J. Phys. Chem. B* **1998**, *102*, 1013−1020.
(64) Andersson, A.; Ahl, Å.; Eklund, R.; Widmalm, G.; Mäler, L. *J. Biomol. NMR* **2005**, *31*, 311−320.
(65) Lycknert, K.; Edebrink, P.; Widmalm, G. *Angew. Chem., Int. Ed.* **2004**, *43*, 2288−2290.
(66) Larsson, E. A.; Staaf, M.; Söderman, P.; Höög, C.; Widmalm, G. *J. Phys. Chem. A* **2004**, *108*, 3932−3937.
(67) Peter, C.; Rueping, M.; Wörner, H. J.; Jaun, B.; Seebach, D.; van Gunsteren, W. F. *Chem— Eur. J.* **2003**, *9*, 5838−5849 and references therein.
(68) Lycknert, K.; Edblad, M.; Imberty, A.; Widmalm, G. *Biochemistry* **2004**, *43*, 9647−9654.
(69) Bosshard, H. R. *News Physiol. Sci.* **2001**, *16*, 171−173.
(70) Jansson, P.-E.; Kenne, L.; Widmalm, G. *Anal. Biochem.* **1991**, *199*, 11−17.
(71) Kjellberg, A.; Widmalm, G. *Biopolymers* **1999**, *50*, 391−399.
(72) Kupèe, E.; Boyd, J.; Campbell, I. D. *J. Magn. Reson. B* **1995**, *106*, 300−303.
(73) Geen, H.; Freeman, R. *J. Magn. Reson.* **1991**, *93*, 93−141.
(74) Nishida, T.; Widmalm, G.; Sándor, P. *Magn. Reson. Chem.* **1996**, *34*, 377−382.
(75) Canet, D.; Levy, G. C.; Peat, I. R. *J. Magn. Reson.* **1975**, *18*, 199−204.
(76) Damberg, P.; Jarvet, J.; Gräslund, A. *J. Magn. Reson.* **2001**, *148*, 343−348.
(77) Stejskal, E. O.; Tanner, J. E. *J. Chem. Phys.* **1965**, *42*, 288−292.
(78) Mills, R. *J. Phys. Chem.* **1973**, *77*, 685−688.
(79) Gibbs, S. J.; Johnson, C. S., Jr. *J. Magn. Reson.* **1991**, *93*, 395−402.
(80) Brooks, B. R.; Bruccoleri, R. E.; Olafson, B. D.; States, D. J.; Swaminathan, S.; Karplus, M. *J. Comput. Chem.* **1983**, *4*, 187−217.
(81) MacKerell, A. D., Jr.; Bashford, D.; Bellott, M.; Dunbrack, R. L., Jr.; Evanseck, J. D.; Field, M. J.; Fischer, S.; Gao, J.; Guo, H.; Ha, S.; Joseph-McCarthy, D.; Kushnir, L.; Kuczera, K.; Lau, F. T. K.; Mattos, C.; Michnick, S.; Ngo, T.; Nguyen, T. D.; Prodhom, B.; Reiher, W. E., III; Roux, B.; Schlenkrich, M.; Smith, J. C.; Stote, R.; Straub, J.; Watanabe, M.; Wiórkiewicz-Kuczera, J.; Yin, D.; Karplus, M. *J. Phys. Chem. B* **1998**, *102*, 3586−3616.
(82) Eklund, R.; Widmalm, G. *Carbohydr. Res.* **2003**, *338*, 393−398.
(83) Jorgensen, W. L.; Chandrasekhar, J.; Madura, J. D.; Impey, R. W.; Klein, M. L. J. *J. Chem. Phys.* **1983**, *79*, 926−935.
(84) Hockney, R. W. *Methods Comput. Phys.* **1970**, *9*, 136−211.
(85) Berendsen, H. J. C.; Postma, J. P. M.; van Gunsteren, W. F.; DiNola, A.; Haak, J. R. *J. Chem. Phys.* **1984**, *81*, 3684−3690.
(86) Steinbach, P. J.; Brooks, B. R. *J. Comput. Chem.* **1994**, *15*, 667−683.